Elucidating the factors that cause cation diffusion shutdown in spinel-based electrodes

Sanjeev Krishna Kolli and Anton Van der Ven*

Materials Department, University of California Santa Barbara, Santa Barbara, CA 93106, USA

E-mail: avdv@engineering.ucsb.edu

Abstract

We report on a systematic study of guest cation (i.e. Li, Na or Mg) diffusion within spinel intercalation compounds, a promising class of materials for Li-, Na- and Mg-ion batteries. Using kinetic Monte Carlo simulations, we identify factors that are responsible for a strong concentration dependence of the cation diffusion coefficient. We focus on spinels in which the guest cations prefer the octahedral sites and where diffusion is mediated by vacancy clusters. Starting with Mg_yTiS_2, we predict an abrupt drop in the Mg diffusion coefficient that spans several orders of magnitude around $y \approx 0.5$ due to the onset of highly correlated Mg diffusion. The prediction is consistent with previous experimental studies that are only able to achieve half the theoretical capacity of Mg_yTiS_2. We next perform a parametric study of diffusion in spinels using kinetic Monte Carlo simulations applied to lattice model Hamiltonians and identify a critical topological weakness of the spinel crystal structure that makes it prone to highly correlated cation diffusion at intermediate to high guest cation concentrations. We find that the onset of this highly correlated diffusion becomes more pronounced as the nearest neighbor repulsion between pairs of guest cations becomes stronger, since this increases the dependence of long-range cation diffusion on triple-vacancy clusters.

The results of this study provide guidance with which the concentration dependence of cation diffusion coefficients in spinel can be tailored to reduce the onset of sluggish diffusion at high cation concentrations. The conclusions drawn from this study also apply to other close-packed anion hosts such as disordered rocksalt electrodes and partially ordered spinels.

Introduction

The ability of intercalation compounds to host Li^+, Na^+, K^+ and Mg^{2+} ions has enabled the development of a wide variety of rechargeable battery types that rely on the shuttling of mobile cations between an anode and a cathode.[1–18] The charge and discharge rate of a rechargeable battery is often limited by the diffusion coefficient of the shuttled cation within the electrodes.[19] Cation diffusion coefficients are very sensitive to the crystal structure and chemistry of the electrode material,[20–22] and much effort has been devoted to identifying intercalation compounds with high guest cation mobilities.[23–28] Simple design principles have proven invaluable in the search for new electrode chemistries with superior ion transport coefficients.[25] These design principles, however, are rooted in dilute diffusion theory. Unfortunately, the cation diffusion coefficient often exhibits a strong concentration dependence and can change by orders of magnitude relative to its value in the dilute limit upon the addition of guest cations to the host.[29–39] It is, therefore, desirable to understand how intrinsic chemical and structural features of the host intercalation compound influence the concentration dependence of the guest cation diffusion coefficient.

Today's commercial Li-ion batteries primarily rely on dense transition metal oxides as their cathodes. This includes layered intercalation compounds such as $LiCoO_2$ and its alloyed NMC and NCA variants.[39] Disordered rocksalts are actively studied as promising alternatives to layered compounds due to their higher capacities.[40–44] There has also been a revival of interest in spinel based intercalation compounds, not only for Li ion batteries,[45,46] but also for Na and Mg-ion batteries.[47–53] The anions of most transition metal oxide and sulfide

electrode materials adopt a close-packed, face-centered cubic (fcc) lattice, with transition metals filling a subset of their octahedral interstitial sites.[39] The remaining octahedral and tetrahedral interstitial sites can then be occupied by guest cations such as Li.

The topology of an fcc anion sublattice has important consequences for cation transport. If the mobile cation prefers octahedral sites, it must migrate through a tetrahedral site, where it will usually thermalize, before continuing on to an adjacent octahedral site.[20,30,35,54] Since the intermediate tetrahedral site is coordinated by four octahedral sites, the barriers of cation hops will be sensitive to the number of other cations in the surrounding octahedral sites.[35] Electrostatic and steric interactions make the the migration barrier strongly dependent on the number of cations in surrounding octahedral sites as schematically illustrated in Figure 1. This leads to a diffusion mechanism that is mediated by vacancy clusters such as double vacancies in layered materials[30,32] and triple vacancies in spinels.[20,35] Diffusion by means of vacancy clusters results in highly correlated cation transport and a cation diffusion coefficient that can vary by several orders of magnitude with concentration.[20,30,32,35,38]

In this study, we systematically investigate cation diffusion in intercalation compounds with an fcc anion sublattice, focusing in particular on spinel compounds in which guest cations prefer octahedral sites. We use kinetic Monte Carlo simulations to calculate cation diffusion coefficients and identify the crystallographic and chemical factors that are responsible for the strong concentration dependence of the cation diffusion coefficient in spinels. We start with a study of diffusion in the spinel form of Mg_yTiS_2, which exhibits a capacity that falls short of its theoretical capacity due to sluggish Mg diffusion at high concentrations.[38,52,53] We next perform a parametric study of cation diffusion in spinel to determine the interactions that play the most important role in producing a strong concentration dependence of the diffusion coefficient. The results of this study provide fundamental insights about diffusion in spinel and related disordered rocksalts that should guide the design of electrodes with superior transport properties.

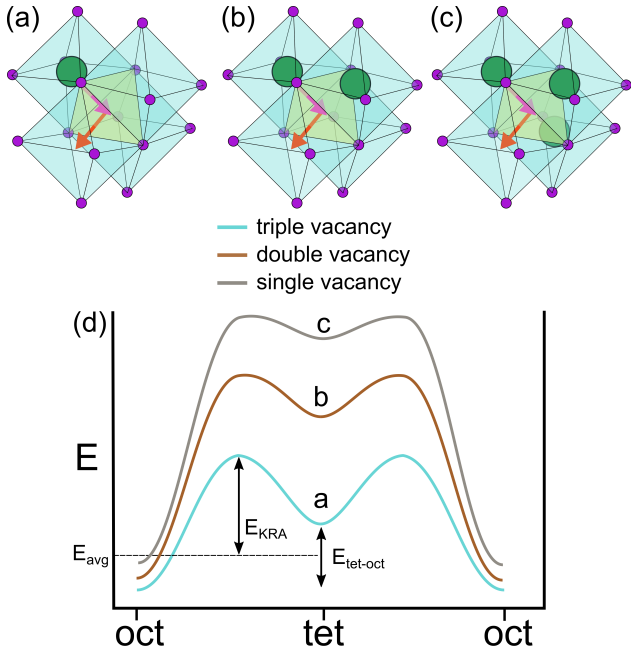

Figure 1: Cation hops between neighboring octahedral sites within an fcc anion sublattice pass through an intermediate tetrahedral site. The intermediate tetraheral site shares faces with four octahedral sites, which makes the migration barrier for a hop between octahedral sites sensitive to the number of other occupied octahedral sites: a triple vacancy hop (a) has a lower barrier than a double vacancy hop (b), which has a lower barrier than a single vacancy hop (c). Purple circles are anions that form the fcc sublattice and green circles are guest cations.

Mg diffusion in spinel TiS_2: the curse of correlated diffusion

We start with a study of cation diffusion in spinel Mg_xTiS_2 since the concentration dependence of its Mg diffusion coefficient is especially pronounced. The promise that Mg-ion batteries can offer high energy densities and capacities due to the 2^+ oxidation state of the shuttled Mg-ions[15,16,55] has led to both theoretical and experimental interest in spinel TiS_2 as a candidate electrode material.[52,56,57] Figure 2 shows the experimentally measured voltage curve of spinel Mg_yTiS_2[38] and compares it to a voltage curve that was calculated with Monte Carlo simulations applied to a first-principles cluster expansion of the Mg_yTiS_2 system at 333 K.[57] The spinel form of TiS_2, which belongs to the $Fd\bar{3}m$ space group, can host Mg in both the 16c octahedral sites and the 8a tetrahedral sites. The cluster expansion approach only accounts for configurational degrees of freedom[19] arising from all the possible ways of distributing Mg cations over the tetrahedral and octahedral sites of the spinel host. The agreement between the measured and calculated voltage curves is very good. Mg predominantly occupies the octahedral sites, but exhibits some tetrahedral site occupancy at intermediate concentrations.[52,57] The smooth voltage curve indicates a solid solution without any strong ordering tendencies.[19]

The experimental voltage curve only extends to $y \approx 0.5$. The calculated voltage curve, in contrast, suggests that the Mg concentration can reach a value of $y \approx 0.8$ before the voltage drops below zero. The limited experimental capacity has been attributed to a decrease in the Mg diffusion coefficient at higher Mg concentrations.[38] Figure 3a shows the self-diffusion coefficient (also referred to as the jump diffusion coefficient[19,58]) of Mg in TiS_2 as calculated with kinetic Monte Carlo simulations at 333 K applied to the same cluster expansion Hamiltonian used to calculate the voltage curve in Figure 2. Migration barriers in the kinetic Monte Carlo simulations were calculated by combining the cluster expansion energies of the end points with a constant kinetically resolved activation (KRA) barrier.[19,30,59–61] The barriers of

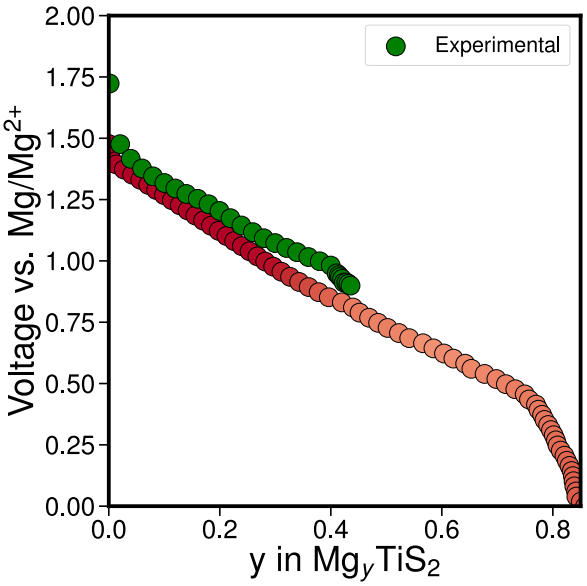

Figure 2: A comparison of the calculated[57] (red) and experimental[38] (green) voltage curve of Mg_yTiS_2. Dark red in the calculated curve signifies octahedral occupancy by Mg, while a lighter shade of red indicates that a fraction of Mg also occupies tetrahedral sites.

hops between octahedral and tetraheral sites are generally found to scale with the difference in the octahedral and tetrahedral site energies.[35] The use of a constant KRA barrier of 0.5 eV was motivated by the results of several density functional theory (DFT) calculations of migration barriers in spinel Mg_yTiS_2 using the nudged elastic band method.[52,62]

The calculated Mg self-diffusion coefficient in Figure 3(a) remains more or less constant below $y = 0.5$, but then decreases by several orders of magnitude in a narrow composition interval. The experimentally measured self-diffusion coefficient by Bonnick *et al.*[38] exhibits a similar variation with composition, although it exhibits a steeper decrease with concentration at dilute Mg concentrations (between $y = 0$ and 0.2) when compared to the calculated diffusion coefficient. Furthermore, the experimental diffusion coefficient only extends to $y \approx 0.5$ due to the onset of strong polarization at higher concentrations. Figure 3(a) clearly reveals a large quantitative discrepancy between the experimental and calculated self-diffusion coefficients. This discrepancy can be attributed to a variety of factors. The extraction of a diffusion coefficient from galvanostatic intermittent titration technique (GITT) measure-

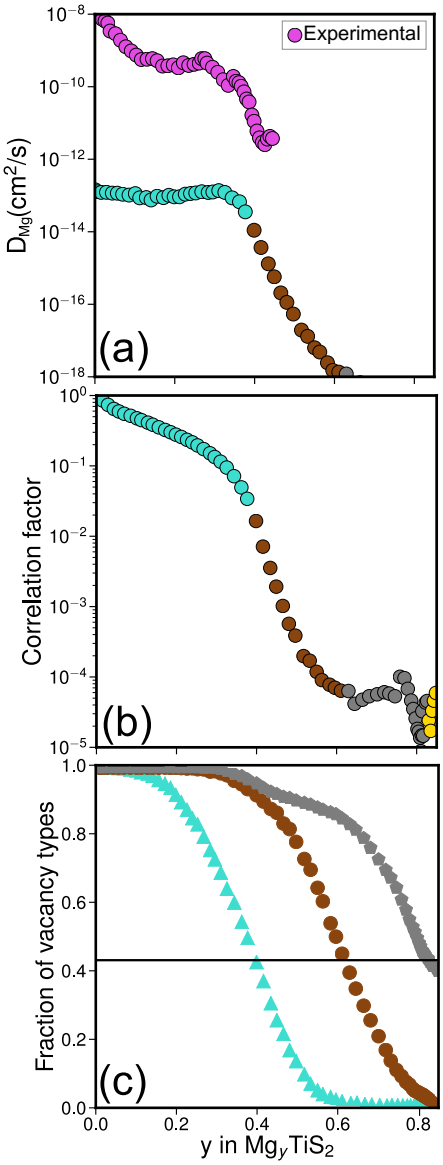

Figure 3: (a) The calculated and experimental[38] self-diffusion coefficients of Mg in Mg_yTiS_2. (b) The calculated correlation factor of Mg in Mg_yTiS_2. (c) The fraction of tetrahedral sites in Mg_yTiS_2 that are surrounded by three or more vacancies (blue), two or more vacancies (brown), and one or more vacancies (grey). The horizontal line is the percolation threshold on the diamond network, the sublattice of the intermediate tetrahedral sites within spinel. The color coding in (a) and (b) signifies the largest vacancy cluster type above the percolation threshold. Yellow points indicate that triple vacancies, double vacancies, and single vacancies are all below the percolation threshold.

ments requires an accurate estimate of the active surface area of the electrode particles,[63] which is often clouded by much uncertainty. Hence the numerical values of reported diffusion coefficients are less reliable than their variation with concentration. The experimental migration barriers as measured in Mg_yTiS_2 are generally more consistent with barriers calculated with DFT[38,52] and, therefore, also more consistent with the lower diffusion coefficients calculated with kMC. Nevertheless, room temperature diffusion coefficients can be very sensitive to errors on the calculated migration barriers, which are typically of the order of 50-100 meV, due to the exponential dependence of hop frequencies on migration barriers.[32] For the purposes of the present discussion, however, only the qualitative variation of the diffusion coefficient with concentration is of primary importance.

Insight about the origin of the sudden drop in the Mg self-diffusion coefficient around $y \approx 0.5$ in Mg_yTiS_2 can be obtained by an inspection of the calculated correlation factor, shown in Figure 3(b). The correlation factor, f, is a measure of the degree with which successive hops are correlated and is equal to 1 when cations perform an unhindered random walk.[19] Any correlations between successive hops will lead to a correlation factor that is less than 1. In general, the tracer diffusion coefficient will be proportional to the correlation factor. Figure 3(b) shows that, similar to the self-diffusion coefficient in Figure 3(a), the calculated correlation factor also decreases by almost four orders of magnitude in a narrow concentration interval around $y \approx 0.5$.

The cause of the sudden onset of highly correlated diffusion can be traced to the diffusion mechanism in Mg_yTiS_2. The kinetic Monte Carlo simulations predict that Mg diffusion in spinel TiS_2 is overwhelmingly dominated by triple vacancy hops. The barriers of triple vacancy hops are much lower than those of the double vacancy and single vacancy hops in Mg_yTiS_2 due to the strong repulsive interaction between a Mg^{2+} cation in an intermediate tetrahedral site and a Mg^{2+} cation in any one of the surrounding octahedral sites that shares a face with the tetrahedral site. Figure 3(c) tracks the fraction of tetrahedral sites with different numbers of vacancies in their four surrounding octahedral sites. The blue curve

in Figure 3(c), for example, collects the fraction of tetrahedral sites that are surrounded by 4 or 3 octahedral vacancies. As is clear in Figure 3(c), the fraction of tetrahedral sites surrounded by 4 or 3 vacancies decreases rapidly with increasing Mg concentration. It is these environments that play a crucial role in mediating Mg transport.

A comparison of Figure 3(b) and Figure 3(c) reveals that the drop in the correlation factor occurs once the triple vacancy concentration dips below the percolation threshold on a diamond network, shown by the horizontal line in Figure 3(c). The tetrahedral sites that constitute the intermediate states between neighboring octahedral sites of the spinel crystal structure form a diamond network.[64] The unhindered diffusion of Mg by means of a triple vacancy mechanism requires a percolating network of quadruple and triple vacancies over this diamond network of tetrahedral sites. Once quadruple and triple vacancies no longer form percolating networks beyond $y \approx 0.5$, the self-diffusion coefficient drops very rapidly and diffusion becomes highly correlated as is evident in Figure 3(a) and (b). Beyond that composition, the kMC simulations predict that the overwhelming majority of Mg hops continue to be mediated by triple vacancies, but the triple vacancies are disconnected and Mg can only migrate back and forth along disconnected chains.

Similar phenomena were predicted for Li diffusion in spinel TiS_2, however, the diffusion coefficient decreases more gradually and at higher concentrations.[35] A crucial difference between Li and Mg diffusion in spinel TiS_2 is the difference in barriers between the triple vacancy mechanism and the double vacancy mechanism. Due to the higher oxidation state of Mg^{2+} cations relative to that of Li^+, the repulsion between two Mg ions occupying adjacent tetrahedral and octahedral sites is larger than that between two Li ions. This leads to double vacancy migration barriers that are significantly higher than those of triple vacancies in Mg_yTiS_2 (roughly 300 meV). For Li the difference in barriers between triple and double vacancy hops is less pronounced (roughly 120 meV). Hence, when the triple vacancy concentration is below the percolation threshold, Li can still escape isolated networks of interconnected triple vacancies with reasonable hop frequencies via double vacancy channels,

even if they constitute a very small minority of the hops. This behavior is also known to occur in metallurgical alloys, where highly correlated diffusion sets in once the lowest barrier hop environment no longer forms percolating chains.[65]

Parametric study of diffusion in spinel intercalation compounds

The Mg_yTiS_2 example highlights the crucial role that vacancy clusters play in mediating guest cation diffusion within a spinel host. This is a direct consequence of the close-packed anion sublattice of spinel, which constrains cation migration to hops between octahedral and tetrahedral sites. Similar vacancy cluster diffusion mechanisms should, therefore, dominate in other intercalation compounds with close-packed anion sublattices such as the disordered rocksalts. To develop a more systematic understanding of diffusion mechanisms in these hosts, we next perform kMC simulations using simple lattice models that capture the essential thermodynamic and kinetic properties of intercalation compounds with close-packed anion sublattices. We continue to focus on spinel, not only for its importance as a common electrode crystal structure, but also because it serves as an idealized model of disordered rocksalts.

Electrochemical properties of spinels

The spinel crystal structure has twice as many non-face sharing octahedral sites (16c sites of the $Fd\bar{3}m$ space group) as non-face sharing tetrahedral sites (8a sites). The tetrahedral sites form a diamond network while the octahedral sites reside between pairs of tetrahedral sites. Each tetrahedral site is coordinated by four octahedral sites, while each octahedral site is coordinated by two tetrahedral sites. The network of tetrahedral and octahedral sites in spinel are shown in Figure 4.

Guest cations within spinel will generally have a preference for either the tetrahedral

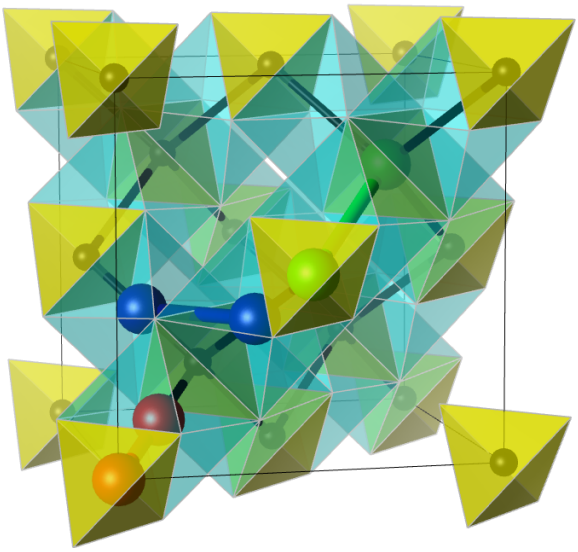

Figure 4: The tetrahedral 8a and octahedral 16c sites of the spinel host, which has the $Fd\bar{3}m$ space group. The corners of the yellow tetrahedra and the turquoise octahedra are anion positions. The tetrahedral sites form a diamond network indicated by the black atoms and bonds. Also shown are the pair clusters that appear in the lattice model Hamiltonian of this study (orange-red balls define a nearest neighbor tetrahedra-octahedral pair, dark blue balls define an octahedral-octahedral pair and light green balls define the tetrahedral-tetrahedral pair).

site or the octahedral site. This site preference is determined by a difference in the energy ΔE_{t-o} between the tetrahedral and the octahedral site. A positive (negative) ΔE_{t-o} signifies an octahedral (tetrahedral) site preference. We can also introduce a nearest neighbor pair interaction between an adjacent pair of octahedral and tetrahedral sites V_{t-o}. This interaction, when positive, describes a repulsion between two guest cations when they occupy a nearest neighbor pair of tetrahedral and octahedral sites. Additional interactions can further refine the model, such as an interaction between nearest neighbor octahedral sites, V_{o-o}, and an interaction between nearest neighbor tetrahedral sites, V_{t-t}, along with other multi-site terms and longer range interactions. The interactions define a lattice model Hamiltonian that can be written as

$$E = \sum_i V_t \sigma_i + \sum_j V_o \sigma_j + \sum_{i,j} V_{t-o} \sigma_i \sigma_j + \dots \tag{1}$$

where the σ_i and σ_j represent occupation variables assigned to each tetrahedral site i and octahedral site j within the crystal (σ_i is equal to 1 when a guest cation occupies site i and zero when the site is vacant). The coefficients V_o and V_t are equal to the dilute site energies of the octahedral and tetrahedral sites, respectively, with $\Delta E_{t-o} = V_t - V_o$. The simple lattice model Hamiltonian in Equation (1) lists the first few terms of a more general cluster expansion Hamiltonian.[19,60,66] A representative example of each of the three pair cluster types of the Hamiltonian are shown in Figure 4. The expansion coefficients of a cluster expansion can be trained to a database of first-principles energies for a large number of different cation vacancy orderings. The resultant Hamiltonian then describes the energy of a particular chemistry as a function of cation-vacancy orderings.[56,57,67] Instead of focusing on a particular chemistry, we next study simple lattice model Hamiltonians parametrically to understand how different interaction coefficients affect thermodynamic and cation-transport properties.

To first order, only two independent interaction parameters are needed to predict commonly observed experimental voltage curves exhibited by spinel compounds. These are the site preference energy parameter ΔE_{t-o} and the nearest-neighbor octahedral-tetrahedral pair interaction V_{t-o}. Figure 5 maps out the regions in ΔE_{t-o} and V_{t-o} space corresponding to qualitatively distinct voltage profiles for the spinel host. The voltage curves were calculated with grand canonical Monte Carlo simulations applied to the simple lattice model Hamiltonian over a grid of ΔE_{t-o} and V_{t-o} values. Four regions with distinct voltage profiles are evident in Figure 5. The site occupancy is shown by the shade of color in the voltage curve, with blue (red) reflecting tetrahedral (octahedral) occupancy and white signifying mixed occupancy.

For positive ΔE_{t-o}, where the octahedral sites are energetically preferred, cation insertion is predicted to proceed through a solid solution, as reflected by the smooth sloping voltage profile.[19] The guest cations gradually fill the octahedral sites until they are completely filled at $y = 1$. Thermal excitations will lead to some degree of tetrahedral site occupancy when

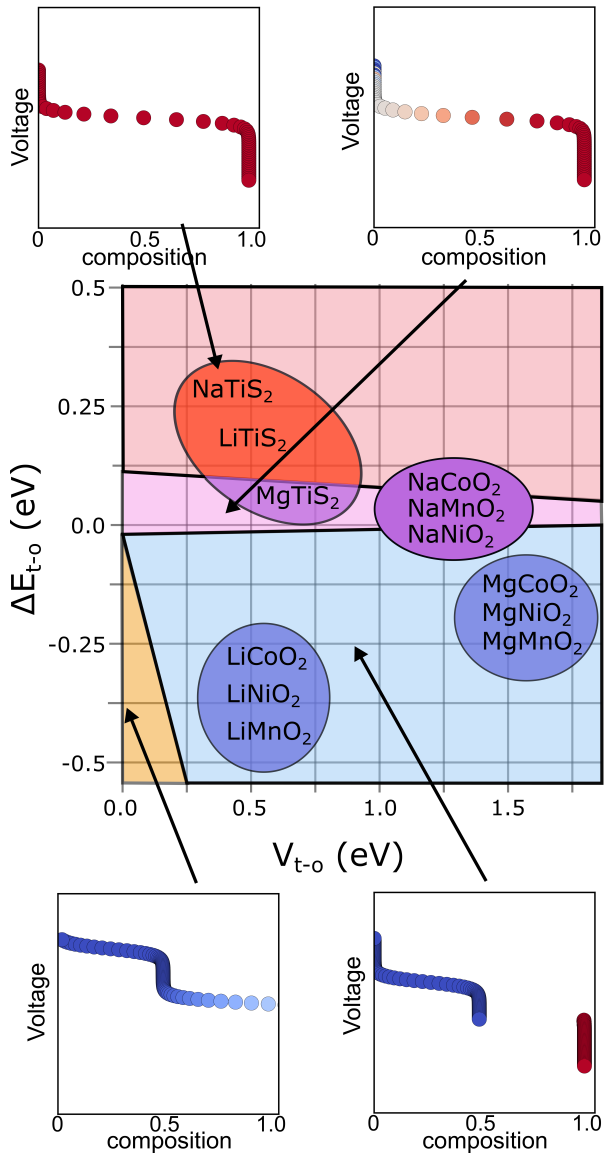

Figure 5: A map of distinct spinel voltage curves as a function ΔE_{t-o}, the difference in energy between tetrahedral and octahedral occupancy, and V_{t-o}, the nearest neighbor pair interaction. The map is based on Monte Carlo simulations performed on a simple, two-parameter lattice model. Rough estimate of where different spinel chemistries lie in this map.

ΔE_{t-o} is small but still positive, reflecting host and guest chemistries where tetrahedral and octahedral sites are close in energy. The nearest neighbor V_{t-o} interaction has little effect on the voltage curves when octahedral sites are preferred.

Negative values of ΔE_{t-o} correspond to a tetrahedral site preference. In this case, the tetrahedral sites fill first until they are completely saturated at x=1/2. Beyond that point the less favorable, but more numerous, octahedral sites must be filled. This leads to a voltage step at $y = 1/2$, as a certain energy is needed to overcome ΔE_{t-o} before octahedral sites can be filled. The qualitative shape of the voltage curve depends on the value of the nearest neighbor V_{t-o} pair interaction. When V_{t-o} is small or negligible, guest cations will simply fill the octahedral sites as a solid solution beyond $y = 1/2$ without displacing tetrahedral cations, as the simultaneous occupation of nearest neighbor tetrahedral and octahedral sites is easily tolerated. However, when V_{t-o} becomes large and positive, nearest neighbor tetrahedral-octahedral pairs become too costly for simultaneous occupancy and the filling of the more numerous octahedral sites is accompanied by a displacement of tetrahedral cations. This is predicted to occur through a two-phase reaction as is evident by the plateau in the voltage curve between $y = 1/2$ and $y = 1$.

More complex insertion sequences emerge upon the addition of longer-range and multi-site interactions to the lattice model Hamiltonian.[34,35,56,57,67–69] For example, the inclusion of a strong repulsion between nearest neighbor octahedral sites, V_{o-o}, when ΔE_{t-o} is positive but not too large will lead to an increase in tetrahedral site occupancy at guest cation concentrations of $y \approx 0.4$. A mix of octahedral and tetrahedral occupancy at intermediate concentrations allows for an increase in the spacing between cations, and thereby a minimization of occupied nearest neighbor octahedral-octahedral pairs to avoid the repulsive V_{o-o} interactions. If the repulsive V_{o-o} interactions are larger than ΔE_{t-o}, then mixed occupancy can be expected, as the penalty of occupying unfavorable tetrahedral sites is smaller than having nearest neighbor octahedral-octahedral occupancy. This occurs in systems such as Mg_yTiS_2,[52] where the strong electrostatic interactions due to the high oxidation state of

the Mg^{2+} leads to a large V_{o-o} pair interaction.[57] Other examples of the effect of additional interactions on the voltage profile and site occupancy are shown in supporting information.

Figure 5 also shows a first-order estimate of where we expect different spinel and guest cation chemistries to fall in the low-dimensional ΔE_{t-o} and V_{t-o} parameter space. The placement of each chemistry in this map should be viewed as an approximate projection from a much higher dimensional parameter space and was guided by the results of past studies using density functional theory calculations.[67] The smaller guest cations such as Li and Mg tend to prefer tetrahedral sites in the more ionic oxide spinel hosts. Since Mg has a higher oxidation state than Li, its nearest neighbor V_{t-o} interaction coefficient will be larger than that for Li. In a sulfide spinel such as TiS_2, which is more covalent than the oxide spinels, guest cations prefer the octahedral sites. The tetrahedral sites are penalized when the guest cation is large, as is the case for Na. Na insertion into an oxide spinel, therefore, results in a ΔE_{t-o} that is close to zero, with tetrahedral and octahedral sites having similar energies. In the TiS_2 spinel, however, the energy of occupying a tetrahedral site is significantly higher than in an octahedral site.

To capture many of the subtle nuances exhibited by each individual chemistry, it is necessary to include many more interaction parameters that extend beyond the site and nearest neighbor pair interaction.[67] These additional interaction terms capture the effects of rehybridization that accompanies transition metal redox[56,70] and lattice parameter changes with guest cation concentration. Furthermore, a system such as $MgCr_2O_4$ has a voltage profile that is more complex than those of Figure 5 due to strong Mg-vacancy ordering tendencies, which are only stabilized by long-range and multi-body interactions.[69] Other spinels such as $MgMn_2O_4$ are susceptible to site inversion, whereby Mn migrates to the sites otherwise available for Mg, depending on its oxidation state.[71,72] This possibility is not accounted for in the lattice model Hamiltonians used to construct the voltage map in Figure 5. Nevertheless, many of the essential features of the chemistries placed in Figure 5 are already captured with a two-interaction parameter lattice model Hamiltonian.

Guest cation diffusion in spinels

Having mapped out how the thermodynamic properties of spinel intercalation compounds depend on the interaction coefficients of a simple lattice model Hamiltonian, we next explore how guest cation diffusion is affected by the interaction coefficients. The Mg_yTiS_2 example shows that the self-diffusion coefficient drops by several orders of magnitude once the triple vacancy concentration falls below the percolation threshold of the diamond network of tetrahedral 8a sites. This behavior is undesirable for battery applications. It occurs because the migration barriers for double vacancy and single vacancy hops are significantly higher than the barriers for triple vacancy hops. Once the concentration of triple vacancies falls below the percolation threshold, the cations are trapped in disconnected chains of triple vacancies. In order to escape, they must migrate into double vacancy or single vacancy clusters, which will only occur to a sufficient degree if the barriers for these hops are not significantly higher than those of hops into triple vacancies. To first order, the barriers associated with different vacancy clusters can be tuned by varying V_{t-o}, the interaction between nearest neighbor tetrahedral and octahedral sites. We explored the effect of variations of the interaction parameters on diffusion coefficients with kinetic Monte Carlo simulations, calculating barriers using a constant KRA of 0.5 eV and evaluating the energies of the end points of the hops with the lattice model Hamiltonian of Equation (1). The concentration dependence of the diffusion coefficient when normalized by the diffusion coefficient at $y = 0$ is relatively insensitive to the value of the KRA as shown in Supporting Information.

We first consider a scenario where V_{t-o} is zero and $\Delta E_{t-o} > 0$. Octahedral sites are then favored, but the energy of the tetrahedral site is unaffected by the number of occupied nearest neighbor octahedral sites. The migration barriers of the triple vacancy, double vacancy and single vacancy hops are then all identical. The calculated self-diffusion coefficient and accompanying correlation factor are shown in Figure 6(a) and (b). The self-diffusion coefficient D is normalized by the self-diffusion coefficient in the dilute limit D_o (i.e. as $y \to 0$). The self-diffusion coefficient decreases with increasing cation concentration y at a rate that

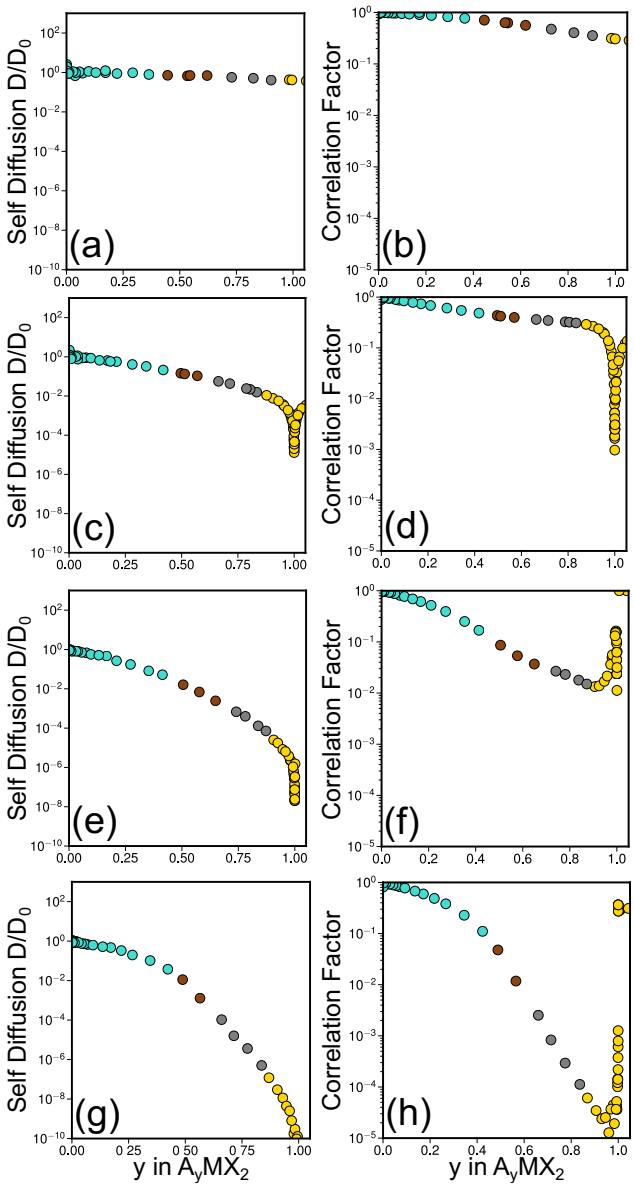

Figure 6: The self diffusion coefficient (also referred to as jump diffusion coefficient) and the correlation factor as calculated with kinetic Monte Carlo for the two-parameter lattice model Hamiltonian for different nearest neighbor pair interactions V_{t-o}: (a-b)$V_{t-o} = 0$ eV, (c-d)$V_{t-o} = 0.1$ eV, (e-f)$V_{t-o} = 0.25$ eV, and (g-h) $V_{t-o} = 0.75$ eV. Points are colored depending on the largest vacancy cluster size above the diamond percolation threshold. In all cases, $\Delta E_{t-o} = 0.0625$.

is proportional to $(1 - y)$ (i.e. the concentration of octahedral vacancies), as expected for the self-diffusion coefficient of an ideal solid solution in which the migration barriers for each hop environment are identical.[73]

Figure 6(c) and (d) show the calculated transport coefficients and correlation factor for a slightly positive V_{t-o}. In this case there is a difference between the triple-vacancy, double vacancy and single vacancy migration barriers. The difference is not too large (relative to k_BT where k_B is Boltzmann's constant and T is the absolute temperature), and double vacancy hops are still accessible. While the majority of hops are mediated by triple-vacancies, once the concentration of quadruple and triple vacancies falls below the percolation threshold, cations are nevertheless still able to escape from isolated triple-vacancy chains by hopping into double vacancies. Hence the correlation factor does not drop precipitously in a narrow concentration interval and the diffusion coefficients do not vary more than one to two orders of magnitude with concentration.

A significant concentration dependence in the self-diffusion coefficient emerges when V_{t-o} is positive and large. Figure 6(e)-(h) shows that the calculated transport coefficients then decrease more significantly with increasing guest cation concentration y. The decrease is especially pronounced in Figure 6(g) and (h) where the self-diffusion coefficient and the correlation factor begin to drop by multiple orders of magnitude once the triple vacancy concentration dips below the percolation threshold in spinel. The decrease, however, is not as abrupt as predicted for Mg_yTiS_2.

We next explore the effect of adding a repulsive interaction between nearest neighbor octahedral sites, V_{o-o}. We consider two scenarios. The first is for a small ΔE_{t-o} (0.0625 eV), which leads to a small difference in energy between tetrahedral and octahedral site occupancy. In this case, a positive V_{o-o} leads to some degree of tetrahedral site occupancy between $y = 0.3$ and $y = 0.6$ as shown in Figure 7(a) and described in the previous section. The second scenario is for a larger ΔE_{t-o} (0.1875 eV), which is chosen sufficiently large to suppress any appreciable tetrahedral occupancy even with a positive V_{o-o} (Figure 7(b)).

The calculated diffusion coefficients and correlation factors for both scenarios are shown in Figure 7(c) - (f). In both cases, there is a dramatic drop in both the self-diffusion coefficient and the correlation factor over a very narrow concentration interval, which is significantly more pronounced than in the cases without a V_{o-o} interaction. The curves for the two scenarios with positive V_{o-o} are very similar in spite of the fact that there is significant tetrahedral site occupancy in the first scenario and almost none in the second (Figure 7(a) and (b)). This suggests that the effect of tetrahedral site occupancy (to the extent predicted for the first scenario) on transport coefficients is not especially large. Instead, it is a positive V_{o-o} that leads to an increase in correlated motion over a narrow concentration interval around the percolation threshold of triple vacancies. A positive V_{o-o} further constricts the diffusion of cations as it will bias hops to octahedral sites that do not have occupied nearest neighbor octahedral sites. These become increasingly rare with increasing cation concentration.

Discussion

The results of this study show that the guest cation diffusion coefficient of an intercalation compound with a close-packed anion sublattice can drop abruptly at intermediate to high cation concentrations, a property that is undesirable for battery applications. Cation diffusion in a host with a close-packed anion sublattice occurs through a succession of hops between octahedral and tetrahedral sites. When cations prefer octahedral sites, they must pass through higher energy tetrahedral sites as they migrate through the crystal. In spinel, these tetrahedral sites are four-fold coordinated. This topological feature of the close-packed anion sublattice leads to a cation diffusion mechanism that is mediated by vacancy clusters, primarily triple vacancies but also a small fraction of double vacancies. This is because the migration barrier, which scales with the tetrahedral site energy, is strongly affected by the number of other cations that occupy adjacent octahedral sites: The barrier to hop into a triple vacancy is lower than that of hopping into a double vacancy, which is itself lower than

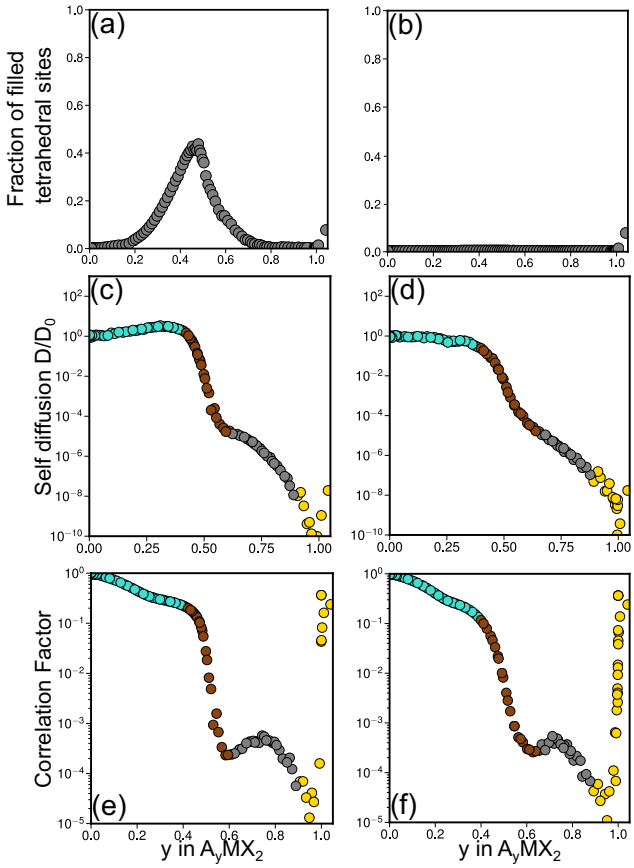

Figure 7: Site preference, self-diffusion coefficients and correlation factors for as predicted with a lattice model Hamiltonian with three parameters (ΔE_{t-o}, V_{t-o} and V_{o-o}). The fraction of tetrahedral sites for (a) a small ΔE_{t-o} (0.0625 eV) and (b) a large ΔE_{t-o} (0.1875 eV). The diffusion coefficient for (c) a small ΔE_{t-o} and (d) a large ΔE_{t-o}. The correlation factor for (e) a small ΔE_{t-o} and (f) a large ΔE_{t-o}. For all cases, $V_{t-o} = 0.75eV$ and $V_{o-o} = 0.083eV$ Points are colored based on the largest vacancy cluster that has a concentration above the percolation threshold. Yellow points indicate no vacancy cluster is above the percolation threshold.

the barrier to hop into a single vacancy (Figure 1). The decrease in triple and double vacancy concentrations with guest cation concentration, therefore, results in a decrease in the cation diffusion coefficient.

Our kinetic Monte Carlo simulations on model spinel systems have revealed that the degree to which the cation diffusion coefficient decreases with cation concentration y depends on the strength of the nearest neighbor repulsion between guest cations. In the absence of a nearest-neighbor repulsion (i.e. $V_{t-o} = 0$), the migration barrier is independent of the hop environment (i.e. the migration barriers for the triple vacancy, double vacancy and single vacancy hops are all identical) and the self-diffusion coefficient scales as $(1 - y)$. Once a repulsion between cations in nearest neighbor octahedral and tetrahedral sites is turned on, the migration barriers for triple vacancy, double vacancy and single vacancy hops begin to differ. The stronger this nearest neighbor repulsion, the larger the differences between the migration barriers of the triple, double and single vacancy hops. This results in a self-diffusion coefficient that decreases more rapidly with y than $(1 - y)$ as is evident in Figure 6(b)-(d).

While the concentration of vacancy clusters has an influence on the cation diffusion coefficient, the kMC simulations for spinel show that this influence manifests itself in a significant way only after the concentration of diffusion mediating defects falls below the percolation threshold of a diamond network, the network of the tetrahedral 8a sites in spinel. It is at this point that the correlation factor can decrease by several orders of magnitude due to highly correlated and, therefore, sluggish cation diffusion. When the nearest-neighbor repulsion is large, the difference in the migration barrier of a triple vacancy and a double vacancy hop is large and diffusion is dominated almost exclusively by triple vacancies. Once the fraction of quadruple and triple vacancies surrounding tetrahedral sites falls below the percolation threshold at approximately $y \approx 0.5$, cation diffusion becomes primarily restricted to disconnected chains of quadruple and triple vacancies. This severely reduces the mobility of the guest cations, as manifested by a rapid decrease in the self-diffusion coefficient. The

decrease in the self-diffusion coefficient becomes even more abrupt upon turning on a repulsive interaction between nearest neighbor octahedral sites (V_{o-o}) as this further restricts the trajectories of cations, causing a sudden decrease in the correlation factor. In Mg_yTiS_2, the effect is especially pronounced and leads to a four orders of magnitude drop in the self-diffusion coefficient around $y \approx 0.5$. In contrast, when the barriers to hop into double vacancies are not much larger than those of hopping into triple vacancies, diffusing cations are more often able to escape disconnected chains of quadruple and triple vacancies, and the decrease in the diffusion coefficient is not as severe. This appears to be the case for Li_yTiS_2, where the decrease in the Li diffusion coefficient is not as sudden and dramatic as that of Mg in Mg_yTiS_2.[35]

We note that the general insights developed here have been distilled from simple lattice model Hamiltonians. Due to their simplicity, they are unable to accurately describe changes in interactions among guest cations that arise from rehybridization that occurs as a result of TM redox and variations in lattice parameters with guest cation concentration.[56,70,74] In general the addition of guest cations to a host material is accompanied by an increase in volume, which tends to lead to lower activation barriers.[20,30,32,35] This effect will partially counter act the predicted decreases in diffusion coefficients with guest cation concentration, however, it is unlikely to significantly affect the concentration dependence of the correlation factor.

Our results suggest ways in which the concentration dependence of the cation diffusion coefficient can be tuned in hosts with close-packed anion sublattices. The key is to modify the strength of the nearest neighbor repulsion between cations that simultaneously occupy adjacent tetrahedral and octahedral sites. This nearest neighbor repulsion is strongly affected by the oxidation state of the cation. For example, Li^+ and Mg^{2+} have approximately the same ionic radii but a different oxidation state, leading to different intercalation behavior that arises from differences in the strength of repulsive interactions due to their oxidation state.[67,75] The study of Bonnick *et al.* of Li_yTiS_2 and Mg_yTiS_2 clearly showed a significant

difference between the Li and Mg diffusion coefficients that is consistent with the predictions of this work.[38] The nearest neighbor repulsion can also be screened to some extent by using larger and more covalent anions, such as sulfur instead of oxygen. Furthermore, the ionic versus covalent nature of the close-packed anion host likely has an effect on the nearest neighbor interaction and can be tuned with transition metal chemistry.[67]

Although we have only explicitly simulated diffusion in spinel hosts, many of the results and conclusions are likely to be relevant for Li diffusion in disordered rocksalts, which also have an fcc anion sublattice. There is currently much interest in disordered rocksalts as candidate electrodes for Li-ion batteries.[40–44] These have a chemical formula of $Li_xM_{1-x}O$ where M refers to a mixture of transition metals. Diffusion in disordered rocksalts is complicated by the random distribution of transition metal cations of the octahedral sites of an fcc oxygen sublattice.[76] A key objective in the optimization of Li transport in a disordered rocksalt is to maximize the number of fully percolating chains of tetrahedral sites that do not share faces with transition metal cations.[40,76] These tetrahedral sites, referred to as 0-TM sites, have lower migration barriers than the tetrahedral sites that share faces with one or two transition metal sites, labeled 1-TM and 2-TM sites, respectively.[40,76] Optimal Li transport occurs in disordered rocksalts with transition metal compositions that ensure percolating networks of 0-TM, which requires a Li:TM ratio greater than 1:1.[40]

The spinel host can be viewed as an idealization of the disordered rocksalts in that its transition metal ordering over the octahedral sites of the fcc anion sublattice ensures fully percolating 0-TM tetrahedral sites. Hence, in contrast to disordered rocksalts, the spinel host does not suffer from a lack of fully percolating 0-TM tetrahedral sites. Nevertheless, spinel does exhibit a strong concentration dependence in the cation self-diffusion coefficient that is very sensitive to a second type of percolation threshold, that of the diffusion mediating vacancy clusters. We expect that this second percolation threshold should also play an important role in disordered rocksalts as it also has an fcc anion sublattice.

Similar to perfectly ordered spinel with octahedral site preference, we expect a decrease

in the Li diffusion coefficient of a disordered rocksalt at high concentrations due to the onset of highly correlated diffusion once the concentration of low barrier vacancy clusters fall below a percolation threshold. The percolation threshold of disordered rocksalts, however, is likely to differ from that of perfectly ordered spinel. The TM depletion of Li-excess disordered rocksalts may open up more 0-TM tetrahedral sites and produce a more disordered sublattice of 0-TM sites when compared to the diamond network of 0-TM sites in spinel. An increase in the connectivity of the 0-TM network will lower the percolation threshold above which the concentration of quadruple and triple vacancies must be kept to maintain fully interconnected chains of favorable diffusion pathways. Generally the percolation threshold can be reduced by increasing the coordination number of each site of a particular network. For example, the percolation threshold of diamond, which has a coordination number of 4, is 0.4286, while those of bcc and fcc, which have coordination numbers of 8 and 12, are 0.2458 and 0.1994, respectively.[64] Hence, the cation disorder in disordered rocksalts[40,42] and disordered spinels[46] may offer opportunities to introduce more interconnected networks of 0-TM sites compared to that of perfect spinel, and thereby make it possible to avoid significant drops in the diffusion coefficients at high Li concentrations. The disorder among transition metal cations and the increased concentration of available octahedral sites in Li-excess disordered rocksalts is also likely to affect the difference in migration barriers for triple, double and single vacancy hops. The extent to which this is the case can be investigated with first-principles electronic structure calculations.

Conclusion

We have systematically studied cation diffusion in intercalation compounds with an fcc anion sublattice, with a particular focus on the spinel structure. An fcc anion sublattice constrains guest cation diffusion to successive hops between octahedral and tetrahedral sites, which leads to a diffusion mechanism that is predominantly mediated by vacancy clusters at

non-dilute cation concentrations. This type of diffusion becomes highly correlated at high guest cation concentrations, especially when the concentration of the diffusion mediating vacancy cluster falls below a percolation threshold. We have shown that the effect becomes more pronounced as the difference in migration barriers between triple, double and single vacancy hops increases. While our study explicitly focused on cation diffusion in spinel, these insights should also apply to other compounds with close-packed anion-sublattices, including disordered rocksalts and partially ordered spinels.

Methods

Density Functional Theory (DFT) as parametrized by Perdew, Burke and Ernzerhoff (PBE)[77] was used to calculate formation energies of Mg-vacancy orderings over the interstitial sites of spinel TiS_2. DFT calculations were performed using the Vienna ab-initio simulation package (VASP).[78,79] Projector augmented wave (PAW)[80,81] theory was used to treat the core electrons. A plane-wave cutoff energy of 450 eV was used along with a k-point density of 32 Å. Formation energies of Mg-vacancy configurations over the tetrahedral and octahedral sites of spinel TiS_2 were used to train a cluster expansion Hamiltonian[66,82] to predict the energy of arbitrary configurations within spinel TiS_2.[57] The cluster expansion Hamiltonian was used in grand canonical and kinetic Monte Carlo simulations to calculate room temperature electrochemical properties, including open circuit voltage profiles, equilibrium site occupancies, diffusion coefficients and correlation factors. The Clusters Approach to Statistical Mechanics (CASM) software package[60,83–85] was used to construct and parametrize the cluster expansions and to perform the grand canonical and kinetic Monte Carlo simulations. The migration barriers within the kinetic Monte Carlo simulations were calculated by combining the cluster expansion for the end states of hops with a constant kinetically resolved activation (KRA) barrier as described elsewhere.[19,30,59] A KRA value of 0.5 eV was used, which was motivated by calculations of barriers of dilute Mg configurations within a 2x2x2

supercell of the primitive spinel-TiS_2 cell and by barriers calculated at non-dilute concentration.[52] Transition state theory[86] was used to calculate hop frequencies within kinetic Monte Carlo simulations. A vibrational prefactor of the hop frequency was set equal to 5 x 10^{12} Hz. Kinetic Monte Carlo simulations were used to calculate Onsager transport coefficients, self-diffusion coefficients and the correlation factor.[19]

Supporting Information: lattice model Hamiltonian parameters, corresponding diffusion quantities for values of these parameters outside those shown in the main text, NEB barriers, extra comparisons, and variation of diffusion quantities as a function of KRA,

Acknowledgements

This material is based on work funded by the National Science Foundation Grant Number OAC-2004693. We acknowledge support from the Center for Scientific Computing from the CNSI, MRL, an NSF MRSEC (Grant DMR-1121053). This research used resources of the National Energy Research Scientific Computing Center, a DOE Office of Science User Facility supported by the Office of Science of the U.S. Department of Energy under Contract DE-AC02-05CH11231.

References

(1) Whittingham, M. S. Electrical energy storage and intercalation chemistry. *Science* **1976**, *192*, 1126–1127.

(2) Mizushima, K.; Jones, P.; Wiseman, P.; Goodenough, J. B. LixCoO2 (0¡ x¡-1): A new cathode material for batteries of high energy density. *Materials Research Bulletin* **1980**, *15*, 783–789.

(3) Goodenough, J.; Thackeray, M.; David, W.; Bruce, P. Lithium insertion into manganese spinels. *Mater. Res. Bull* **1983**, *18*, 461–472.

(4) Thackeray, M.; Johnson, P.; De Picciotto, L.; Bruce, P.; Goodenough, J. Electrochemical extraction of lithium from LiMn2O4. *Materials Research Bulletin* **1984**, *19*, 179–187.

(5) Dahn, J. Phase diagram of Li x C 6. *Physical Review B* **1991**, *44*, 9170.

(6) Tarascon, J.; Wang, E.; Shokoohi, F.; McKinnon, W.; Colson, S. The spinel phase of LiMn2 O 4 as a cathode in secondary lithium cells. *Journal of the Electrochemical Society* **1991**, *138*, 2859.

(7) Tarascon, J.; Guyomard, D. The Li1+ xMn2O4/C rocking-chair system: a review. *Electrochimica Acta* **1993**, *38*, 1221–1231.

(8) Whittingham, M. S. Lithium batteries and cathode materials. *Chemical reviews* **2004**, *104*, 4271–4302.

(9) Goodenough, J. B.; Park, K.-S. The Li-Ion Rechargeable Battery: A Perspective. *Journal of the American Chemical Society* **2013**, *135*, 1167–1176, PMID: 23294028.

(10) Delmas, C.; Braconnier, J.-J.; Fouassier, C.; Hagenmuller, P. Electrochemical intercalation of sodium in NaxCoO2 bronzes. *Solid State Ionics* **1981**, *3*, 165–169.

(11) Yabuuchi, N.; Kubota, K.; Dahbi, M.; Komaba, S. Research development on sodium-ion batteries. *Chemical reviews* **2014**, *114*, 11636–11682.

(12) Delmas, C. Sodium and sodium-ion batteries: 50 years of research. *Advanced Energy Materials* **2018**, *8*, 1703137.

(13) Kim, H.; Kim, J. C.; Bianchini, M.; Seo, D.-H.; Rodriguez-Garcia, J.; Ceder, G. Recent progress and perspective in electrode materials for K-ion batteries. *Advanced Energy Materials* **2018**, *8*, 1702384.

(14) Hosaka, T.; Kubota, K.; Hameed, A. S.; Komaba, S. Research development on K-ion batteries. *Chemical reviews* **2020**, *120*, 6358–6466.

(15) Yoo, H. D.; Shterenberg, I.; Gofer, Y.; Gershinsky, G.; Pour, N.; Aurbach, D. Mg rechargeable batteries: an on-going challenge. *Energy & Environmental Science* **2013**, *6*, 2265–2279.

(16) Canepa, P.; Sai Gautam, G.; Hannah, D. C.; Malik, R.; Liu, M.; Gallagher, K. G.; Persson, K. A.; Ceder, G. Odyssey of multivalent cathode materials: open questions and future challenges. *Chemical reviews* **2017**, *117*, 4287–4341.

(17) Koketsu, T.; Ma, J.; Morgan, B. J.; Body, M.; Legein, C.; Dachraoui, W.; Giannini, M.; Demortière, A.; Salanne, M.; Dardoize, F., et al. Reversible magnesium and aluminium ions insertion in cation-deficient anatase TiO 2. *Nature materials* **2017**, *16*, 1142–1148.

(18) Bai, Q.; Yang, L.; Chen, H.; Mo, Y. Computational studies of electrode materials in sodium-ion batteries. *Advanced energy materials* **2018**, *8*, 1702998.

(19) Van der Ven, A.; Deng, Z.; Banerjee, S.; Ong, S. P. Rechargeable alkali-ion battery materials: theory and computation. *Chemical reviews* **2020**, *120*, 6977–7019.

(20) Van der Ven, A.; Bhattacharya, J.; Belak, A. A. Understanding Li Diffusion in Li-Intercalation Compounds. *Accounts of Chemical Research* **2013**, *46*, 1216–1225, PMID: 22584006.

(21) Islam, M. S.; Fisher, C. A. Lithium and sodium battery cathode materials: computational insights into voltage, diffusion and nanostructural properties. *Chemical Society Reviews* **2014**, *43*, 185–204.

(22) Deng, Z.; Mo, Y.; Ong, S. P. Computational studies of solid-state alkali conduction in rechargeable alkali-ion batteries. *NPG Asia Materials* **2016**, *8*, e254–e254.

(23) Gardiner, G. R.; Islam, M. S. Anti-site defects and ion migration in the LiFe0. 5Mn0. 5PO4 mixed-metal cathode material. *Chemistry of Materials* **2010**, *22*, 1242–1248.

(24) Liu, M.; Rong, Z.; Malik, R.; Canepa, P.; Jain, A.; Ceder, G.; Persson, K. A. Spinel compounds as multivalent battery cathodes: a systematic evaluation based on ab initio calculations. *Energy & Environmental Science* **2015**, *8*, 964–974.

(25) Rong, Z.; Malik, R.; Canepa, P.; Sai Gautam, G.; Liu, M.; Jain, A.; Persson, K.; Ceder, G. Materials design rules for multivalent ion mobility in intercalation structures. *Chemistry of Materials* **2015**, *27*, 6016–6021.

(26) Wood, S. M.; Eames, C.; Kendrick, E.; Islam, M. S. Sodium ion diffusion and voltage trends in phosphates Na4M3 (PO4) 2P2O7 (M= Fe, Mn, Co, Ni) for possible high-rate cathodes. *The Journal of Physical Chemistry C* **2015**, *119*, 15935–15941.

(27) Liu, M.; Jain, A.; Rong, Z.; Qu, X.; Canepa, P.; Malik, R.; Ceder, G.; Persson, K. A. Evaluation of sulfur spinel compounds for multivalent battery cathode applications. *Energy & Environmental Science* **2016**, *9*, 3201–3209.

(28) Rong, Z.; Xiao, P.; Liu, M.; Huang, W.; Hannah, D. C.; Scullin, W.; Persson, K. A.; Ceder, G. Fast Mg 2+ diffusion in Mo 3 (PO 4) 3 O for Mg batteries. *Chemical Communications* **2017**, *53*, 7998–8001.

(29) Kanehori, K.; Kirino, F.; Kudo, T.; Miyauchi, K. Chemical diffusion coefficient of lithium in titanium disulfide single crystals. *Journal of the Electrochemical Society* **1991**, *138*, 2216.

(30) Van der Ven, A.; Ceder, G.; Asta, M.; Tepesch, P. First-principles theory of ionic diffusion with nondilute carriers. *Physical Review B* **2001**, *64*, 184307.

(31) Jang, Y.-I.; Neudecker, B. J.; Dudney, N. J. Lithium diffusion in Li x CoO2 (0.45¡ x¡ 0.7) intercalation cathodes. *Electrochemical and Solid State Letters* **2001**, *4*, A74.

(32) Van der Ven, A.; Thomas, J. C.; Xu, Q.; Swoboda, B.; Morgan, D. Nondilute diffusion from first principles: Li diffusion in Li x TiS 2. *Physical Review B* **2008**, *78*, 104306.

(33) Yang, S.; Wang, X.; Yang, X.; Bai, Y.; Liu, Z.; Shu, H.; Wei, Q. Determination of the chemical diffusion coefficient of lithium ions in spherical Li [Ni0. 5Mn0. 3Co0. 2] O2. *Electrochimica Acta* **2012**, *66*, 88–93.

(34) Bhattacharya, J.; Van der Ven, A. Phase stability and nondilute Li diffusion in spinel Li 1+ x Ti 2 O 4. *Physical Review B* **2010**, *81*, 104304.

(35) Bhattacharya, J.; Van der Ven, A. First-principles study of competing mechanisms of nondilute Li diffusion in spinel Li_xTiS_2. *Phys. Rev. B* **2011**, *83*, 144302.

(36) Delacourt, C.; Ati, M.; Tarascon, J. Measurement of lithium diffusion coefficient in Li y FeSO4F. *Journal of the Electrochemical Society* **2011**, *158*, A741.

(37) Belak, A. A.; Wang, Y.; Van der Ven, A. Kinetics of anatase electrodes: the role of ordering, anisotropy, and shape memory effects. *Chemistry of Materials* **2012**, *24*, 2894–2898.

(38) Bonnick, P.; Sun, X.; Lau, K.-C.; Liao, C.; Nazar, L. F. Monovalent versus Divalent Cation Diffusion in Thiospinel Ti$_2$S$_4$. *The Journal of Physical Chemistry Letters* **2017**, *8*, 2253–2257.

(39) Radin, M. D.; Hy, S.; Sina, M.; Fang, C.; Liu, H.; Vinckeviciute, J.; Zhang, M.; Whittingham, M. S.; Meng, Y. S.; Van der Ven, A. Narrowing the gap between theoretical and practical capacities in Li-ion layered oxide cathode materials. *Advanced Energy Materials* **2017**, *7*, 1602888.

(40) Lee, J.; Urban, A.; Li, X.; Su, D.; Hautier, G.; Ceder, G. Unlocking the potential of cation-disordered oxides for rechargeable lithium batteries. *science* **2014**, *343*, 519–522.

(41) Yabuuchi, N.; Takeuchi, M.; Nakayama, M.; Shiiba, H.; Ogawa, M.; Nakayama, K.; Ohta, T.; Endo, D.; Ozaki, T.; Inamasu, T., et al. High-capacity electrode materials for

rechargeable lithium batteries: Li3NbO4-based system with cation-disordered rocksalt structure. *Proceedings of the National Academy of Sciences* **2015**, *112*, 7650–7655.

(42) Clément, R.; Lun, Z.; Ceder, G. Cation-disordered rocksalt transition metal oxides and oxyfluorides for high energy lithium-ion cathodes. *Energy & Environmental Science* **2020**, *13*, 345–373.

(43) Liu, H.; Zhu, Z.; Yan, Q.; Yu, S.; He, X.; Chen, Y.; Zhang, R.; Ma, L.; Liu, T.; Li, M., et al. A disordered rock salt anode for fast-charging lithium-ion batteries. *Nature* **2020**, *585*, 63–67.

(44) Lun, Z. et al. Cation-disordered rocksalt-type high-entropy cathodes for Li-ion batteries. *Nature Materials* **2021**, *20*, 214–221.

(45) Manthiram, A.; Chemelewski, K.; Lee, E.-S. A perspective on the high-voltage LiMn 1.5 Ni 0.5 O 4 spinel cathode for lithium-ion batteries. *Energy & Environmental Science* **2014**, *7*, 1339–1350.

(46) Ji, H. et al. Ultrahigh power and energy density in partially ordered lithium-ion cathode materials. *Nature Energy* **2020**, *5*, 213–221.

(47) Kim, J.; Amatucci, G. Structural and electrochemical investigation of Na+ insertion into high-voltage spinel electrodes. *Chemistry of Materials* **2015**, *27*, 2546–2556.

(48) Kim, J.; Amatucci, G. NaMn2-xNixO4 Derived from Mesoporous LiMn2-xNixO4: High-Voltage Spinel Cathode Materials for Na-Ion Batteries. *Journal of the Electrochemical Society* **2016**, *163*, A696.

(49) Vasileiadis, A.; Carlsen, B.; de Klerk, N. J.; Wagemaker, M. Ab initio study of sodium insertion in the λ-Mn2O4 and dis/ordered λ-Mn1. 5Ni0. 5O4 spinels. *Chemistry of Materials* **2018**, *30*, 6646–6659.

(50) Canepa, P.; Bo, S.-H.; Gautam, G. S.; Key, B.; Richards, W. D.; Shi, T.; Tian, Y.; Wang, Y.; Li, J.; Ceder, G. High magnesium mobility in ternary spinel chalcogenides. *Nature communications* **2017**, *8*, 1–8.

(51) Canepa, P.; Sai Gautam, G.; Broberg, D.; Bo, S.-H.; Ceder, G. Role of point defects in spinel Mg chalcogenide conductors. *Chemistry of Materials* **2017**, *29*, 9657–9667.

(52) Sun, X.; Bonnick, P.; Duffort, V.; Liu, M.; Rong, Z.; Persson, K. A.; Ceder, G.; Nazar, L. F. A high capacity thiospinel cathode for Mg batteries. *Energy & Environmental Science* **2016**, *9*, 2273–2277.

(53) Bonnick, P.; Blanc, L.; Vajargah, S. H.; Lee, C.-W.; Sun, X.; Balasubramanian, M.; Nazar, L. F. Insights into Mg2+ Intercalation in a Zero-Strain Material: Thiospinel Mg x Zr2S4. *Chemistry of Materials* **2018**, *30*, 4683–4693.

(54) Van der Ven, A.; Ceder, G. Lithium diffusion mechanisms in layered intercalation compounds. *Journal of power sources* **2001**, *97*, 529–531.

(55) Sun, X.; Bonnick, P.; Nazar, L. F. Layered TiS2 positive electrode for Mg batteries. *ACS Energy Letters* **2016**, *1*, 297–301.

(56) Emly, A.; Van der Ven, A. Mg intercalation in layered and spinel host crystal structures for Mg batteries. *Inorganic chemistry* **2015**, *54*, 4394–4402.

(57) Kolli, S. K.; Van der Ven, A. First-principles study of spinel MgTiS2 as a cathode material. *Chemistry of Materials* **2018**, *30*, 2436–2442.

(58) Gomer, R. Diffusion of adsorbates on metal surfaces. *Reports on Progress in Physics* **1990**, *53*, 917–1002.

(59) Van der Ven, A.; Ceder, G. First principles calculation of the interdiffusion coefficient in binary alloys. *Physical review letters* **2005**, *94*, 045901.

(60) Van der Ven, A.; Thomas, J. C.; Puchala, B.; Natarajan, A. R. First-principles statistical mechanics of multicomponent crystals. *Annual Review of Materials Research* **2018**, *48*, 27–55.

(61) Goiri, J. G.; Kolli, S. K.; Van der Ven, A. Role of short- and long-range ordering on diffusion in Ni-Al alloys. *Phys. Rev. Materials* **2019**, *3*, 093402.

(62) Kolli, S. K.; der Ven, A. V. Supporting Information for "Elucidating the factors that cause cation diffusion shutdown in spinel-based electrodes". **2021**,

(63) Weppner, W.; Huggins, R. A. Determination of the kinetic parameters of mixed-conducting electrodes and application to the system Li3Sb. *Journal of The Electrochemical Society* **1977**, *124*, 1569.

(64) van der Marck, S. C. Percolation thresholds and universal formulas. *Physical Review E - Statistical Physics, Plasmas, Fluids, and Related Interdisciplinary Topics* **1997**, *55*, 1514–1517.

(65) Van der Ven, A.; Yu, H.-C.; Ceder, G.; Thornton, K. Vacancy mediated substitutional diffusion in binary crystalline solids. *Progress in Materials Science* **2010**, *55*, 61–105.

(66) Sanchez, J.; Ducastelle, F.; Gratias, D. Generalized Cluster Description of Multicomponent Systems. *Physica A: Statistical Mechanics and its Applications* **1984**, *128*, 334–350.

(67) Kolli, S. K.; Van Der Ven, A. Controlling the Electrochemical Properties of Spinel Intercalation Compounds. *ACS Applied Energy Materials* **2018**, *1*, 6833–6839.

(68) Wagemaker, M.; Van Der Ven, A.; Morgan, D.; Ceder, G.; Mulder, F.; Kearley, G. Thermodynamics of spinel LixTiO2 from first principles. *Chemical Physics* **2005**, *317*, 130–136.

(69) Chen, T.; Sai Gautam, G.; Huang, W.; Ceder, G. First-principles study of the voltage profile and mobility of Mg intercalation in a chromium oxide spinel. *Chemistry of Materials* **2018**, *30*, 153–162.

(70) Van der Ven, A.; Aydinol, M.; Ceder, G.; Kresse, G.; Hafner, J. First-principles investigation of phase stability in Li x CoO 2. *Physical Review B* **1998**, *58*, 2975.

(71) Sai Gautam, G.; Canepa, P.; Urban, A.; Bo, S.-H.; Ceder, G. Influence of inversion on Mg mobility and electrochemistry in spinels. *Chemistry of Materials* **2017**, *29*, 7918–7930.

(72) Tuerxun, F.; Otani, S.; Yamamoto, K.; Matsunaga, T.; Imai, H.; Mandai, T.; Watanabe, T.; Uchiyama, T.; Kanamura, K.; Uchimoto, Y. Phase Transition Behavior of MgMn2O4 Spinel Oxide Cathode during Magnesium Ion Insertion. *Chemistry of Materials* **2021**, *33*, 1006–1012.

(73) Kutner, R. Chemical diffusion in the lattice gas of non-interacting particles. *Physics Letters A* **1981**, *81*, 239–240.

(74) Kaboudvand, F.; Vinckeviciute, J.; Kolli, S.; Radin, M. D.; Van der Ven, A. Phase Stability and Electronic Structure of Tin Sulfide Compounds for Li-ion Batteries. *The Journal of Physical Chemistry C* **2019**, *123*, 29086–29095.

(75) Radin, M. D.; Van der Ven, A. Stability of prismatic and octahedral coordination in layered oxides and sulfides intercalated with alkali and alkaline-earth metals. *Chemistry of Materials* **2016**, *28*, 7898–7904.

(76) Urban, A.; Lee, J.; Ceder, G. The configurational space of rocksalt-type oxides for high-capacity lithium battery electrodes. *Advanced Energy Materials* **2014**, *4*, 1400478.

(77) Perdew, J. P.; Burke, K.; Ernzerhof, M. Generalized Gradient Approximation Made Simple. *Physical Review Letters* 3865–3868.

(78) Kresse, G.; Furthmüller, J. Efficient Iterative Schemes For\italicsab Initio Total-Energy Calculations Using a Plane-Wave Basis Set. *Physical Review B* 11169–11186.

(79) Kresse, G.; Furthmüller, J. Efficiency of Ab-Initio Total Energy Calculations for Metals and Semiconductors Using a Plane-Wave Basis Set. *Computational Materials Science* 15–50.

(80) Blöchl, P. E. Projector Augmented-Wave Method. *Physical Review B* 17953–17979.

(81) Kresse, G.; Joubert, D. From Ultrasoft Pseudopotentials to the Projector Augmented-Wave Method. *Physical Review B* 1758.

(82) DeFontaine, D. Cluster Approach to Order-Disorder Transformations in Alloys. *Solid State Physics* 33–176.

(83) Puchala, B.; Van der Ven, A. Thermodynamics of the Zr-O system from first-principles calculations. *Physical review B* **2013**, *88*, 094108.

(84) Thomas, J. C.; Van der Ven, A. Finite-temperature properties of strongly anharmonic and mechanically unstable crystal phases from first principles. *Physical Review B* **2013**, *88*, 214111.

(85) CASM Developers, CASM, v0.2.1. Available from https:// github.com/prisms-center/CASMcode, 2018.

(86) Vineyard, G. H. Frequency factors and isotope effects in solid state rate processes. *Journal of Physics and Chemistry of Solids* **1957**, *3*, 121–127.

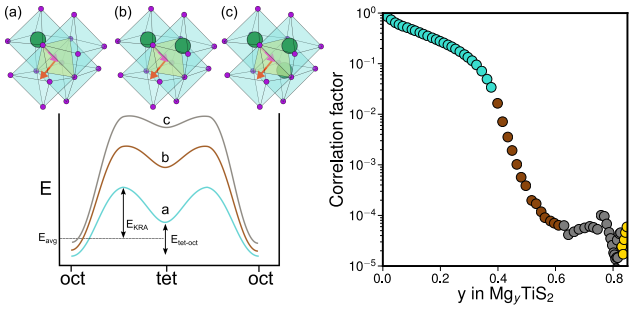
(a)
(b)
(c)
c
b
a
E
E_{KRA}
E_{avg}
$E_{tet-oct}$
oct
tet
oct
Correlation factor
10^{0}
10^{-1}
10^{-2}
10^{-3}
10^{-4}
10^{-5}
0.0
0.2
0.4
0.6
0.8
y in Mg_yTiS_2

TOC Figure